IEEE Access
Multidisciplinary | Rapid Review | Open Access Journal

Date of publication xxxx 00, 0000, date of current version xxxx 00, 0000.

Digital Object Identifier 10.1109/ACCESS.2023.DOI

Linear parameter-varying and fixed-parameter H_∞-based control of a bearingless compressor

ANDREI ZHURAVLEV[1], ATTE PUTKONEN[1], SADJAD MADANZADEH[1], AND RAFAL P. JASTRZEBSKI[2,1] (SENIOR MEMBER, IEEE).

[1]Department of Electrical Engineering, Lappeenranta–Lahti University of Technology LUT, 53850 Lappeenranta, Finland
[2]Department of Mechanical and Materials Engineering, University of Turku, 20014 Turku, Finland

Corresponding author: Andrei Zhuravlev (e-mail: andrei.zhuravlev@lut.fi).

This work was supported by Business Finland: "EMBER High-temperature high-efficiency oil-free heat pump," no. 1745/31/2020, Tohtoristipendi 2021 at LUT, Suomen Kulttuurirahasto grant no. 00211193, and the Academy of Finland under grant no. 350880.

ABSTRACT

Bearingless machines have the potential to provide shorter rotors and achieve overall lower losses and higher energy densities than traditional technologies. However, levitation control has to overcome some further challenges. The aim of this work is to attain robust levitation in the presence of disturbances of various nature. To address dynamics dependent on varying speed, a linear parameter-varying (LPV) H_∞-based control of magnetic suspension is applied, where speed is the scheduled parameter. The model-based centralized position control uses an inverse nonlinearity compensation and position estimation at actuator locations to decouple levitation and motoring as well as to linearize the plant model. Different control configurations and resulting performances are benchmarked from the application perspective. The tested controllers are synthesized according to the same weighting scheme. However, the control synthesis is achieved by using a Linear Matrix Inequality and a Riccati-based algorithm. A fixed-parameter H_∞ controller and an LPV controller are evaluated against a gain uncertainty. The performance of the controllers is studied based on frequency-domain analysis and time-domain simulations against accurate nonlinear plant models derived by Finite Element Modeling. Analytical results, supported by simulations with a detailed nonlinear plant model, together with selected experimental tests, assist the evaluation of the control performance of a 160 kW bearingless two-stage compressor prototype. The compressors serve as part of a 500 kW high-temperature industrial heat pump.

INDEX TERMS H_∞ robust control, linear parameter-varying (LPV), bearingless rotor, magnetic levitation, non-collocation, heat pump, high-speed compressor

I. INTRODUCTION

EMERGING high-speed kinetic compressor applications respond to global sustainability strategies that aim to minimize the industrial carbon footprint and enable low-carbon society technologies. One notable example is compressors used in industrial heat pumps and chillers. The continuous search for further increases in efficiency and energy density leads to further-increasing differences in operating temperatures of heat pumps and speeds of compressors. However, high-speed rotors with magnetic bearings face rotor dynamics issues (resulting from the increased length), an increased component count, and larger footprints. A new paradigm of the high-speed compressor has been the centralization of the bearing and torque production functionality in a bearingless rotor.

Bearingless machines have gained significant attention in the past few decades due to their numerous advantages, such as reduced friction, increased efficiency, and extended service life. Potential use-cases for bearingless motors in large industrial systems were reviewed in [1]. The largest experimentally tested machine at nominal power was demonstrated by Liu et al. [2] at 60 kW for a twin unit. However, reports on higher power laboratory experimental machines do not provide experimental results in nominal conditions, e.g., [3], [4], pointing to control challenges at higher speeds.

Precise and robust control of the rotor suspension system

ensuring stable levitation and preventing contact between the rotor and the stator is a critical aspect of bearingless machine operation. Various model-based and proportional–integral–derivative (PID)-based active levitation control strategies have been proposed and implemented for bearingless machines [5], [6]. From the mechanical point of view, the rotor levitation control shares similarities with the active magnetic bearing (AMB) rotor control. These examples include both centralized and decentralized control solutions. Generally, centralized model-based controllers have demostrated superiority over PID and PD/PI controllers [7].

For the model-based control of active levitation, the H_∞ control is a popular choice owing to its robust performance in the presence of uncertainties and disturbances. It minimizes the worst-case gain from disturbance inputs to regulate the performance outputs, effectively attenuating the impact of the worst disturbances. In the H_∞ framework, various weighting schemes can be applied. In [8], the authors compared an H_∞ controller, built using a signal-based weighting scheme with PID and linear quadratic regulator (LQR) controllers. They show experimentally that an H_∞ controller exhibits considerable robustness against speed variation while using less control current, even though the performance is lower than for the LQR. Further examples of H_∞ controllers synthesized according to the signal-based and loop-shaping performance weighting schemes applied to AMB rotors are given in [9]. Both analytical and experimental comparisons show that the signal-based approach provides a better robust stability. Further experimental results of applying the H_∞ control to actively suppress vibrations in magnetic actuators are presented in [10]. Importantly, this approach successfully passes the first critical speed.

Linear parameter-varying (LPV) control has been applied to magnetically suspended rotor systems because of its ability to handle varying operating conditions and improve the control performance. Various LPV synthesis approaches have been used, e.g., a Linear Matrix Inequality (LMI) and a Riccati-based algorithm (RIC). The RIC has been proven to provide accurate/robust results, but it can be computationally demanding and, in some cases, may not converge [11]. The LMI approach, on the other hand, often leads to conservative solutions and may not always be applicable, depending on the nature of the control problem [12]. Well-designed AMBs are linear with respect to currents and positions, but the AMB–rotor system, when operating with highly gyroscopic rotors, becomes nonlinear because of the rotational speed. Model predictive control (MPC) based on LPV models was considered for an active magnetic bearing (AMB) system in [13]. System identification and control of a nonlinear electromagnetic actuator with an LPV controller for a levitated system was investigated in [14]. H_∞ LPV approach was applied to semiactive suspension control in [15]. The aim of [16] was to address the effects of mass imbalance disturbances. This was achieved by incorporating a parameter-dependent performance weight into the design of a robust LPV controller. The approach takes account of neglected system dynamics by integrating a fixed additive uncertainty weight. In [17], a switching-based LPV control approach was proposed to obtain a high-performance gain-scheduled control by maintaining continuity of the Lyapunov function across the defined parameter subset boundaries. In [18], and [19], the LPV approach was investigated in the case of highly gyroscopic AMB rotors. Those works focused on the design of H_∞–based stabilizing controllers within variable speeds to cover the full operating region. In [20], a neural network-based model was considered to obtain a velocity-dependent model for the LPV control. As proposed in [21], a generalized interpolation scheme applies LPV-type controllers for AMB-suspended systems, employing Youla–Kucera parametrization. For actuators that maximize the force density, also forces are nonlinear with respect to currents and displacements. An LMI-based controller with a time-varying effective stiffness parameter was used to recover stable operation of the AMB after a contact with the touchdown bearing in [22]. Finally, an active fault-tolerant control for LPV models was effectively applied to an AMB rotor system in [23].

Bearingless rotors are trailing behind the AMB rotors, which are well established for all power levels in industrial applications. While bearingless machines share similarities with magnetic bearing-based solutions, the force production mechanics require the use of a rotating reference frame as well as different application specifics of force–torque decoupling in the controller. Further, the system, electronics, and machine design are significantly more challenging, particularly for shared-winding machines and multi-degree-of-freedom actively suspended rotors, contributing to bridge a research and application gap between AMBs and bearingless rotors.

This work reduces the research gap by significantly extending the results published in [24]. Here, the H_∞ and LPV controls are studied in more detail by providing a comparison of various control strategies and experimental results. Control system design options and a comparison between a fixed-parameter H_∞ control and an LPV H_∞ controller applied to an innovative high-power bearingless compressor are detailed for the first time. The inverse nonlinearity [25] for levitation force decoupling and linearization requires position estimation at nodes related to the actuators. Therefore, estimation of the rotor position at bearing locations, within the H_∞ framework, is proposed. Schemes to obtain rotor positions at bearing locations and different optimal control synthesis methods of the LPV controller best suited for the application are discussed, and the performance of the controllers under varying conditions is analyzed. In the comparison, both the fixed-parameter H_∞ controller and the LPV controller are designed according to the same weighing scheme but using two different synthesis approaches, namely the LMI and the RIC. The RIC-based algorithm allows easier separation of the controller and observer structures capable of estimating the rotor position, including contributions from

estimated rotor bending mode states at bearing locations.

The structure of the paper follows the control design process. It starts with modeling in Section II, which comprises a brief explanation of the modeling methods, a description of the linearized plant model used for control synthesis, and an accurate model used for simulations. Section III follows with an introduction of the adopted control structure, the fixed and variable parameter H_∞ control synthesis. Section IV presents simulated and experimental results and robust performance evaluation. The closed-loop performance is evaluated using frequency-domain analysis and time-domain simulations with a detailed nonlinear plant model. The simulations are validated against experimental results obtained from a heat pump compressor equipped with a bearingless motor, which has been reported, e.g., in [26], [27]. The subsequent multidisciplinary design of a bearingless compressor for a high-temperature industrial heat pump has been presented in [4], [28].

II. MODELING

This section discusses two plant models in brief: a linearized plant model used for controller synthesis and a very accurate nonlinear electromechanical model used to verify the control by Matlab Simulink simulations.

A. PLANT MODEL FOR CONTROL DESIGN

The electromagnetic behavior of the bearingless motor is modeled using the JMAG Finite Element Modeling (FEM) software. Magnetic force models obtained from the FEM exhibit cross coupling, load dependence, and eccentricity dependence, as discussed in [25]. This electromagnetic model is used to compute motor parameters and the contribution of the motoring current to the force production. Coupling of nonlinear terms in the electromagnetic force and torque relations cannot be directly used for the plant formulation. However, owing to inverse nonlinearity compensation, the control plant model can comprise only the mechanical part with added delays caused by the presence of the inner current control loops.

This mechanical model is also built with FEM, which considers Timoshenko beam modeling. The rotor model used for the control plant is a linear model with retained rigid rotor modes and the first (lowest frequency) two rotor bending modes (symmetrical in the xz and in yz planes) after modal decomposition and model reduction.

The noncollocated arrangement of sensors and actuators in the rotor layout is shown in Fig. 1. The real rotor is not symmetrical along the z-axis because of different-sized compressor wheels at low- and high-pressure (LP and HP) ends.

B. PLANT MODEL FOR CONTROL VERIFICATION

A verification model comprises an actuator electromagnetic model and a rotor-dynamic mechanical model. Actuator nonlinear forces F are modeled using a lookup table (LUT) obtained from the FEM results. This LUT comprises xy force vectors as a function of the motor and suspension dq currents and rotor angular position θ. It is supplemented by the analytical nonlinear eccentricity model dependent on the rotor translation positions xy. The accuracy of the LUT can be increased in expense of the FEM simulation time for LUT preparation.

The flexible rotor model with retained three first bending modes, per plane, depicted in Fig. 1, is a reduced Timoshenko beam FEM-derived model. Additionally, runout at sensor locations, unbalance forces, pulse width modulation (PWM), and current saturation are taken into account in the verification model. The block diagram of the closed-loop system is shown in Fig. 2.

III. CENTRALIZED MODEL-BASED CONTROL

The cascaded control structure, presented in Fig. 2, comprises the decentralized inner current control and the outer centralized position control loops. The inner loops have a bandwidth of 2500 Hz, while the outer position control loop is much slower. The inner-loop dynamics are controlled through four two-phase equivalent variables in a rotating reference frame. The outer position loop is regulated with a model-based H_∞ controller in the stationary frame. The outer position control loop provides a control force signal that transforms into the control current through the inverse force mapping and comes as a control input to the inner loop. The inverse force mapping defines the suspension currents that should be produced to obtain the required force at certain radial displacements, angular positions, and motoring currents [25]. This force-linearizing block is extracted from the FEM model and can be represented with an inverted matrix equations or with a pseudo inverse LUT. Both the motor speed control and all the inner current control loops are built on PI controllers. The speed control strategy assumes $i_d = 0$ with a measured rotor position. This is the most energy efficient approach [29], which also simplifies the levitation force modeling and control.

A. FIXED-PARAMETER H_∞ CONTROLLER

Here, we select a signal-based two-degrees-of-freedom weighting scheme (Fig. 3a) for the levitation control synthesis, because the machine physical signal constraints are known. It is a general approach for multivariable problems. Five weights ($\mathbf{W_r}$, $\mathbf{W_n}$, $\mathbf{W_d}$, $\mathbf{W_e}$, $\mathbf{W_u}$) define the frequency characteristics of the exogenous signals affecting the

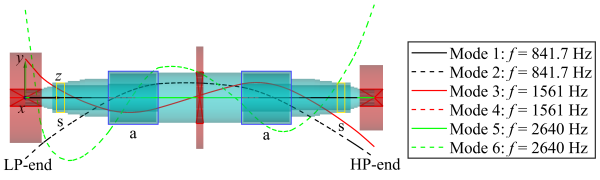

FIGURE 1. FEM rotor model with the first three bending modes. Sensor locations, s; actuator locations, a. LP and HP are the low- and high-pressure ends, respectively.

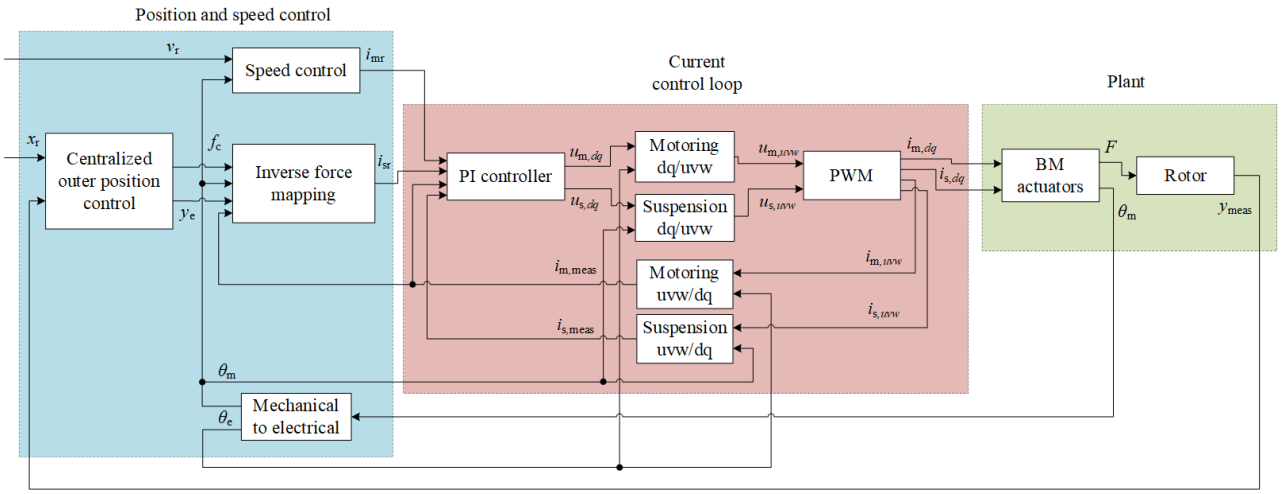

FIGURE 2. Control system architecture comprising the outer position control, the inner current control loops, and the plant. Here, the LUT-based inverse nonlinearity block uses the rotor position, estimated in the controller, at the bearing locations y_e.

system inputs and the desired frequency content of error and system outputs. In practice, these weights are used for the tuning of the controller.

The first problem is reference tracking (servo problem), which is only applied during a start-up from the safety bearings to move the rotor to the center position. The second and the main concern is the control problem with good disturbance attenuation. Disturbances considered here are due to unbalanced forces, noise, and runout at sensor locations. Additional disturbances, which are not explicitly taken into account when making the weight selection, can result from compressor blade dynamics and interactions of flow field dynamics, e.g., due to surge or stall conditions.

The extended closed-loop transfer function of the H_∞ control problem solved with the RIC method is shown in Fig. 3b. The generalized plant $\mathbf{P}$ is based on

$$\begin{cases} \dot{x} = \mathbf{A}x + \mathbf{B_1}w + \mathbf{B_2}u \\ z = \mathbf{C_1}x + \mathbf{D_{11}}w + \mathbf{D_{12}}u. \\ y = \mathbf{C_2}x + \mathbf{D_{21}}w + \mathbf{D_{22}}u \end{cases} \tag{1}$$

Because of noncollocation and the selected inverse nonlinearity linearizing strategy, the sensor feedback and control signals must be converted into the same coordinates. On the one hand, if the sensor measurements are transformed into the bearing coordinates using rigid rotor transformations, the information about the contribution of the bending modes to the displacement is lost. On the other hand, if the rotor position at the bearing locations is derived from the estimator, which does estimate the states of both the rigid and bending rotor modes, the estimation error will propagate into the feedback. Those cases provide us with two alternative methods to obtain the rotor positions at bearing locations needed for the inverse nonlinearity block. The state feedback and observer gains can be formed as

$$\begin{cases} \dot{x}_e = \mathbf{A}x_e + \mathbf{B_1}w_e + \mathbf{B_2}u + \mathbf{L_x}e \\ u = \mathbf{K_u}x_e + \mathbf{L_u}e, \\ w_e = \mathbf{K_w}x_e \end{cases} \tag{2}$$

where w_e is the estimated worst case perturbation, x_e is the estimated state vector, the $\mathbf{K_u}$ and $\mathbf{K_w}$ are the state feedback controller gains, and the $\mathbf{L_x}$ and $\mathbf{L_u}$ are the observer gains. The innovation term is expressed [11], [30] as:

$$e = y - \mathbf{C_2}x_e - \mathbf{D_{21}}w_e - \mathbf{D_{22}}u. \tag{3}$$

The RIC method allows to separate the controller and the estimator and to retain the meaning of the physical state; therefore, the rotor position at the bearing locations $\hat{y}_b$ can be estimated. The output of the matrix $\mathbf{C_2}$ is an estimated rotor position at sensor locations. It should be converted into bearing coordinates with the matrix $\mathbf{C_b}$ as shown in (4). The state–space representation of the controller $\mathbf{K}$ with the estimated output position at the bearing locations is derived from (1) – (3) and yields the system equations in the following form

$$\begin{cases} \dot{x}_e = [\mathbf{A} + \mathbf{B_1}\mathbf{K_w} + \mathbf{B_2}\mathbf{K_u} + (\mathbf{B_2}\mathbf{L_u} + \mathbf{L_x}) \\ \qquad (-\mathbf{C_2} - \mathbf{D_{21}}\mathbf{K_w})]x_e + [\mathbf{B_2}\mathbf{L_u} + \mathbf{L_x}]y \\ u = [\mathbf{K_u} + \mathbf{L_u}(-\mathbf{C_2} - \mathbf{D_{21}}\mathbf{K_w})]x_e + \mathbf{L_u}y, \\ \hat{y}_b = [\mathbf{0_{4x16}} \quad \mathbf{C_b} \quad \mathbf{0_{4x4}}]x_e \end{cases} \tag{4}$$

where $\mathbf{C_b}$ is the output matrix at bearing locations. The order of the states of controller is as follows: 16 states are related to weights, 12 states to the mechanical plant (the states related to the first bending mode are included), and four states to the actuators.

When synthesizing an H_∞ controller, it is important to ensure that the H_∞ problem has solutions and is far from singularity. It is advantageous to synthesize the controller fulfilling the weighted robust performance without adding extra

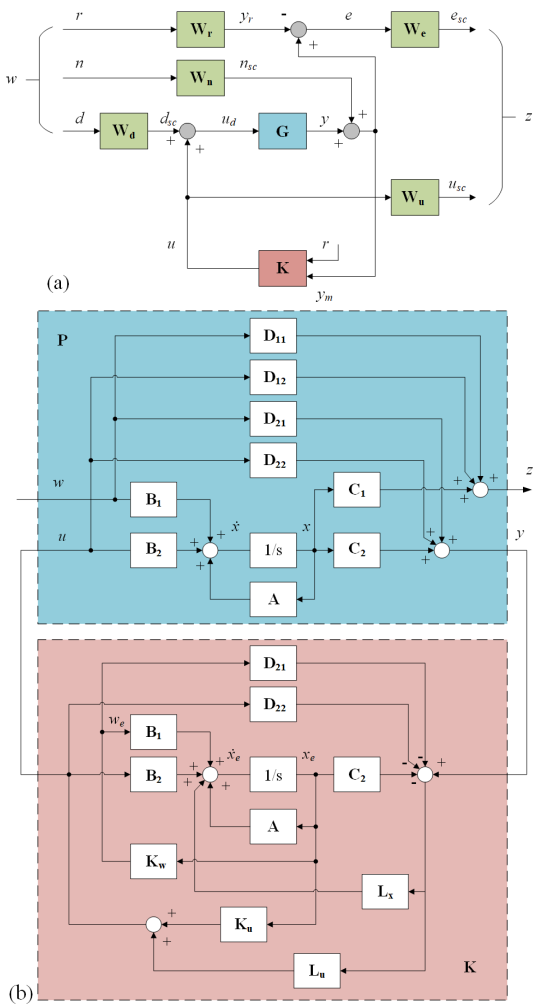

FIGURE 3. (a) Two-degrees-of-freedom H_∞ weighting scheme used in this study. The weights $\mathbf{W_r}$, $\mathbf{W_n}$, $\mathbf{W_d}$, $\mathbf{W_e}$, and $\mathbf{W_u}$ are used to scale the reference, noise, external disturbance, error and control effort, respectively. $\mathbf{G}$ is the plant, and $\mathbf{K}$ the controller. (b) General H_∞ scheme for the controller synthesized with the RIC method with separated state feedback and observer gains, where the physical meaning of the states is retained and an estimation of the rotor position at bearing locations is employed.

states to meet the design objectives. The fewer constraints are set, the easier it is to achieve the convergence of the H_∞ problem, and the resulting controller to be implemented is smaller. Additionally, retaining the physical meaning and the state order is required for the linearization that employs the estimated positions. The fixed-parameter H_∞ controller is synthesized by employing the weights given in Table 1. Four weights are the first-order transfer functions, and one weight is a scalar. $W(0)$ is a DC gain, and $W(\infty)$ is a high-frequency gain. ω_b is the bandwidth defined as the frequency at which the magnitude response is 3 dB (0.707 in absolute values) below the low-frequency gain. The selected design weights reflect the physical signal constraints and lead to the desired properties of the closed-loop system. For example, the noise is 10 % of the maximum measured values; the unbalance disturbances increase in proportion to the rotational speed,

TABLE 1. The values considered in the weighting functions for the H_∞ problem comprise symmetric and diagonal 4x4 matrices.

Filter	Values
$W_r(s)$	$W(0) = 1, W(\infty) = 0.01, \omega_\mathrm{b} = 31.2 \cdot 2\pi$
$W_n(s)$	0.1
$W_d(s)$	$W(0) = 0.065, W(\infty) = 1, \omega_\mathrm{b} = 1.18 \cdot 10^3 \cdot 2\pi$
$W_e(s)$	$W(0) = 2000, W(\infty) = 1, \omega_\mathrm{b} = 0.01 \cdot 2\pi$
$W_u(s)$	$W(0) = 1, W(\infty) = 2, \omega_\mathrm{b} = 96.7 \cdot 2\pi$

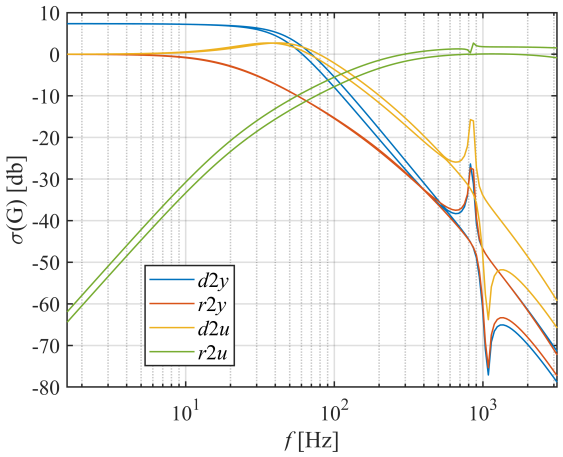

FIGURE 4. Minimum and maximum singular values of four closed-loop transfer functions: disturbance-to-position (d2y), reference-to-position (r2y), disturbance-to-control effort (d2u), and reference-to-control effort (r2u).

and the control effort is physically limited by the actuator characteristics. The nominal bandwidth of the actuators is 2500 Hz. The higher gain at low frequencies and roll-off at high frequencies are targeted for good servo and regulation properties.

The performance is evaluated by singular value analysis, where the selected closed-loop functions are disturbance-to-position (d2y), reference-to-position (r2y), disturbance-to-control effort (d2u), and reference-to-control effort (r2u). The results are depicted in Fig. 4, and they indicate a well-behaving control loop. The control system is four-input four-output (FIFO); the highest singular value of 7.3 db is for d2y at low frequencies. The r2y and d2y transfer functions are critical. The bandwidth for r2y is 20.5 Hz, and for d2y is 42.7 Hz.

B. LPV H_∞ CONTROLLER

The LPV H_∞ control is an extension of the fixed-parameter H_∞ control that is formulated to handle LPV systems.

In terms of broader classification, the LPV systems that use the H_∞ control with a reference model in the weighting scheme can be considered as both the Model Adaptive Control (MAC) and the Model Reference Control (MRC). The LPV H_∞ control is a form of MAC, because the controller adapts to changes in the system parameters. It is also a form of MRC, because a reference model is used to define the

desired rotor position behavior.

In this study, the LPV H_∞ control strategy is adopted to handle the varying speed of the bearingless rotor. Other varying parameters, such as position within the air gap and current amplitudes, are not considered because the dependence of the actuator on those parameters is linearized by the force inverse block. The LPV system is represented by using a polytopic model given by (5), where the vertices of the polytope vary with the speed parameter. The polytopic approach can be used because of the linear dependence on the parameter [31]. Ten vertices are used in the polytope to accurately capture the variation in the speed parameter:

$$\underbrace{\begin{bmatrix}\mathbf{A}(t)+j\mathbf{E}(t) & \mathbf{B}(t)\\ \mathbf{C}(t) & \mathbf{D}(t)\end{bmatrix}}_{\mathbf{S}(t)} \in \in \mathbf{C_O}\left\{\underbrace{\begin{bmatrix}\mathbf{A_1}+j\mathbf{E_1} & \mathbf{B_1}\\ \mathbf{C_1} & \mathbf{D_1}\end{bmatrix}}_{\mathbf{S_1}(t)}, \ldots, \underbrace{\begin{bmatrix}\mathbf{A_k}+j\mathbf{E_k} & \mathbf{B_k}\\ \mathbf{C_k} & \mathbf{D_k}\end{bmatrix}}_{\mathbf{S_k}(t)}\right\} \tag{5}$$

where $\mathbf{S_1}(t)...\mathbf{S_k}(t)$ are vertex systems built for the speed range. The synthesis of the LPV H_∞ controller employs a generalized plant description as follows

$$\begin{cases}\dot{x} = \mathbf{A}(p)x + \mathbf{B_1}(p)w + \mathbf{B_2}u\\ z = \mathbf{C_1}(p)x + \mathbf{D_{11}}(p)w + \mathbf{D_{12}}u\\ y = \mathbf{C_2}x + \mathbf{D_{21}}w + \mathbf{D_{22}}u\end{cases} \tag{6}$$

where p is the scheduling parameter. The difference between the above approach and the gain scheduling approach is the interpolation method, which is used to approximate the controller for parameter values within the polytope. While the fixed-parameter controller is synthesized with the LMI and RIC methods, the LPV H_∞ is computed with the LMI method only. For the controller computed with the LMI algorithm, the inverse force mapping block is fed with measured (and not estimated) rotor positions. This applies to the fixed- and H_∞-parameter controllers.

IV. RESULTS AND PERFORMANCE EVALUATION

A. PERFORMANCE ANALYSIS

The synthesized controllers are evaluated for robustness performance in the closed loop using the LPV plant. The maximum singular values of the closed loops for the fixed-parameter and LPV H_∞ controllers at low and high speeds are compared. The evaluated closed-loop transfer functions are

$$d_{sc} \rightarrow y \qquad \mathbf{G}(\mathbf{I}-\mathbf{KG})^{-1} = \mathbf{GS_i}; \tag{7}$$

$$n_{sc} \rightarrow y \qquad \mathbf{GK}(\mathbf{I}-\mathbf{GK})^{-1} = \mathbf{T_o}; \tag{8}$$

$$d_{sc} \rightarrow u \qquad \mathbf{KG}(\mathbf{I}-\mathbf{KG})^{-1} = \mathbf{T_i}; \tag{9}$$

$$n_{sc} \rightarrow u \qquad \mathbf{G}(\mathbf{I}-\mathbf{GK})^{-1} = \mathbf{GS_o}, \tag{10}$$

where $\mathbf{S_i}$ and $\mathbf{S_o}$ are the input and output sensitivities, respectively, and $\mathbf{T_i}$ and $\mathbf{T_o}$ are the complementary input and output sensitivities, respectively. The fixed-parameter H_∞ controller is derived at low speed (1 RPM), whereas the LPV controller is synthesized at low and high speeds. In Fig. 5, the analytical closed-loop frequency responses of the fixed-parameter H_∞ controller, computed using the LMI and RIC methods, are compared at low and high speeds with the frequency responses of the LPV controller. Gain uncertainty of 5% is taken into account. These plots show that the LPV controller can better attenuate the disturbances entering the measured positions at frequencies close to the rotor bending modes as well as external disturbances at low frequencies. If the fixed-parameter H_∞ controller is computed for higher speeds, its performance decreases when tested in the whole speed range [25], and therefore, that case is not presented here.

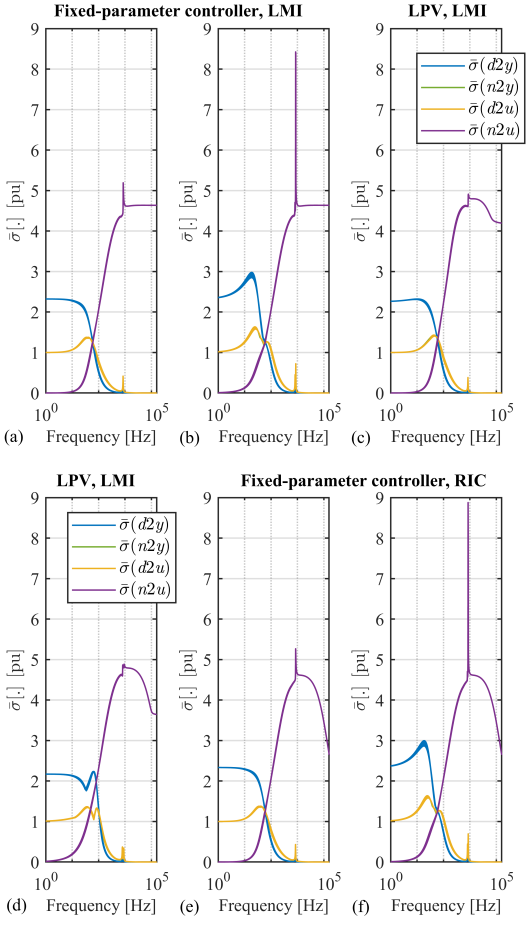

FIGURE 5. Singular values of the closed loops with 5% gain uncertainty for 100 randomized plants for two speed boundary points (0 and 30000 rpm). (a) Using the fixed-parameter H_∞ controller, computed for low speed with the LMI method, tested at low speed. (b) Employing the same controller to the plant at high speed. (c) Using the LPV H_∞ controller, computed for low speed with the LMI method (the recommended method), tested at low speed. (d) Applying the LPV H_∞ controller computed with the LMI method (the recommended method), tested at high speed. (e) Using the fixed-parameter H_∞ controller computed for low speed with the RIC method, tested at low speed. (f) Employing the same H_∞ controller but tested at high speed.

When analyzing the results presented in Fig. 5, it can be seen that the closed-loop system with the controller computed with the RIC method has a roll-off at higher frequencies, while the system with the controller computed with the LMI method has a static gain. It can be noticed that the singular values of the system with the LPV controller are lower at a higher speed, especially in the worst region (the first bending mode). Singular values of the transfer function n2y coincide with d2u. A frequency analysis was conducted for 2, 10, and 100 vertices. The d2y singular values improve with a higher number of vertex systems, while noise-to-control effort becomes slightly worse. The differences are negligible, and therefore, results for a higher number of vertices are not presented here. The FIFO loop system shows a significant stability margin with a disc margin of 0.95, a gain margin of 2.8, and a phase margin of 51 degrees. These metrics ensure robust stability, providing sufficient protection against potential instabilities or disturbances.

In addition to the analytical frequency responses, a time-domain analysis was performed by simulations using the verification plant model described in Section II. The verification plant makes the simulation conditions very close to the actual bearingless compressor.

B. SIMULATION RESULTS

In the simulated event sequence, the acceleration is ramped up from 0 to 30000 RPM during the first 2.8 s, as shown in Fig. 6b. The acceleration rate is chosen based on the currents, ensuring that they stay well below the saturation limit. The nominal design phase current, as well as the inverter limit, is 125 A. The visible position oscillations are mainly caused by runout. An unbalance compensation is applied at 2000 RPM ($\approx$ 1.2 s); it effectively limits the controller responses to the first and second measured position harmonics. The both controllers yield similar position responses, and therefore, Fig. 6a shows the position response of both rotor ends (high and low pressure) during acceleration to the nominal speed only for the system with the fixed-parameter H_∞ controller. A small difference is that the LPV H_∞ controller provides better damping at the speed corresponding to the frequency equal to half of the first bending mode (25251 RPM).The frequency of the first bending mode is 841.7 Hz. The oscillations at this frequency are excited by the second harmonic of runout. When analyzing the suspension and motoring currents in the u-phase of the first bearingless unit shown in Figs. 7a and 7b, it can be seen that the currents do not saturate. Moreover, the system is not highly gyroscopic. For more gyroscopic rotors, the advantage of the LPV controller would, therefore, be more pronounced even for subcritical operation. Nevertheless, in the context of frequency analysis of Fig. 5, the use of the LPV control in the studied bearingless compressor is optimal.

The simulated plant (true) and controller-estimated rotor positions (both observed at bearing locations) of the first bearingless unit in the x-direction, for the controller synthesized with the RIC method, are shown in Fig. 8. The

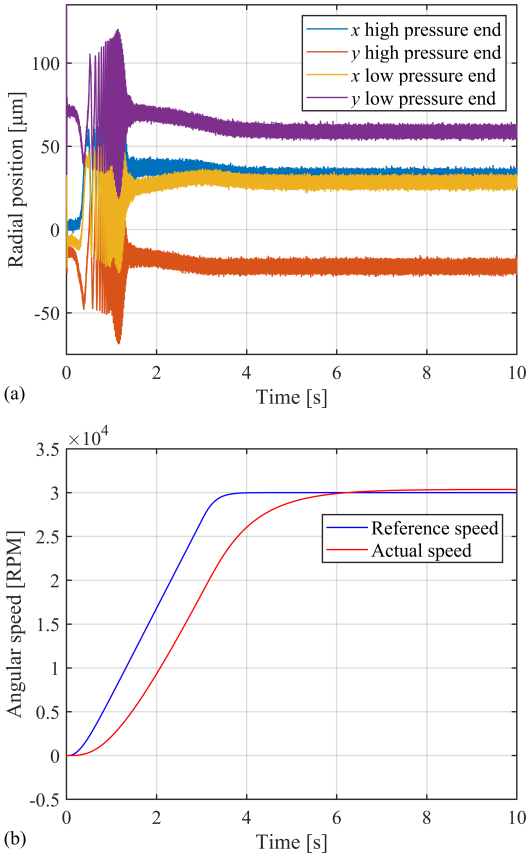

FIGURE 6. (a) Responses of both rotor ends (high and low pressure) during acceleration to the nominal speed. (b) The reference and actual speeds. Main oscillations are caused by runout. However, basic unbalance compensation of the first two harmonics, which is applied at 2000 rpm, effectively limits the oscillations of the outputs.

estimated position is closer to the reference value (that is 0) compared with the simulated positions, resulting in smaller steady-sate errors, and with the measured and transformed positions using rigid body transformation matrices. Moreover, the estimated position has smaller amplitude variations because of the filtering properties of the estimator. Admittedly, the measured and converted positions are closer to the actual plant positions at bearing locations. Nevertheless, using an estimated position as an input to the inverse nonlinearity block provides slightly better overall simulation results than the use of the measured position converted into the bearing coordinates. For measured and converted positions, the information about the phases of the bending modes is potentially compromised depending on the location of the rotor bending mode nodes due to the noncollocation problem.

From inverse nonlinearity (decoupling) linearization method implementation point of view, the LUT approach yields slightly better closed-loop simulated performance compared to the equation based inverse. This is expected because in the LUT the dependence of the force vectors on the rotor angular position is inherently included. However, the LUT based inverse and non inverter plant static models

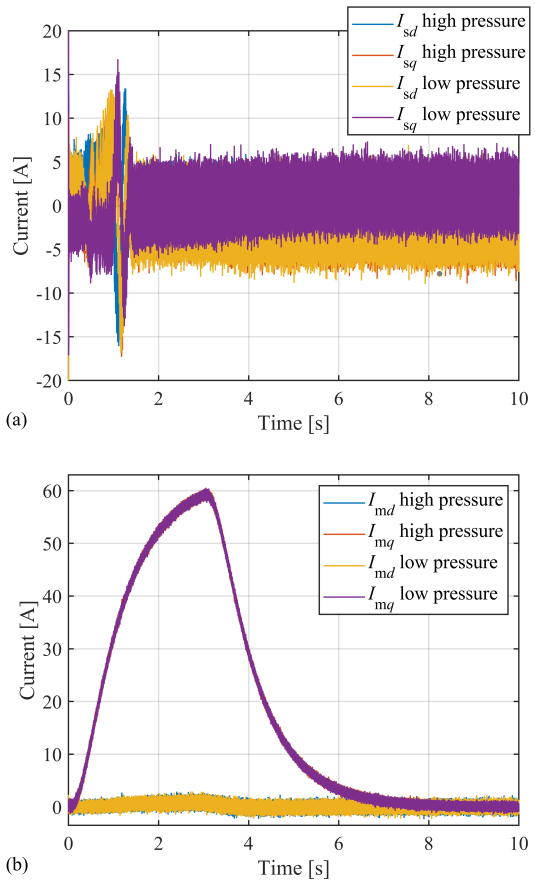

FIGURE 7. (a) Suspension currents in *dq* coordinates, (b) motoring currents in *dq* coordinates.

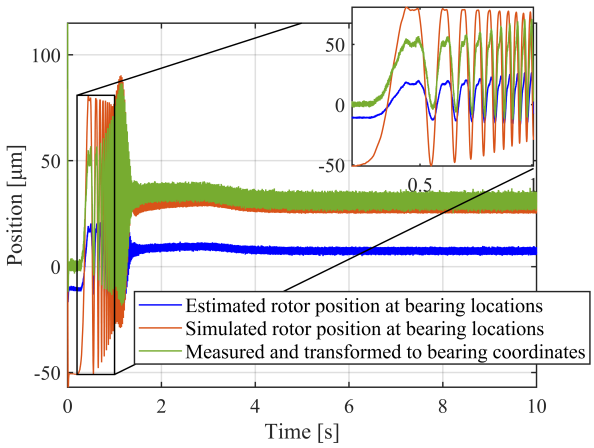

FIGURE 8. Simulated rotor position at bearing locations and measured position transformed into bearing coordinates for the controller synthesized with the RIC method in the x-direction of the high-pressure end.

alike have limitation about FEM computation times and memory for large table implementations. Moreover, in this work, we have not included the torque angle dependence leaving us only with the motor zero i_d current strategy for the motor control.

C. EXPERIMENTAL RESULTS

The prototype machine as in the commissioning stage is shown in Fig. 9. The objective is to verify the modeled and designed controller performances in both the frequency domain and the time domain through start-up tests, ensuring their consistency with the simulated results.

First, the measured and analytical output sensitivity plots of the fixed-parameter H_∞ controller, obtained using 30 μm amplitude excitation to assess the position signals one loop at a time are shown in Fig. 10. The ISO 14839-3:2004(E) lays down acceptable peak output sensitivity values. The sensitivity peaks at 5 dB indicate that the closed-loop system qualifies as one with the best relative stability, operating in zone A with a notable margin for uncertainty according to the standard, before reaching the limit of 9.5 dB. However, the differences at low frequencies between the measured and analytical plots highlight potential modeling errors. Those discrepancies could arise from the inaccurate nonlinearity compensation resulting from inverse LUT errors or errors in rotor positions at bearing locations, estimated or reconstructed from measurements.

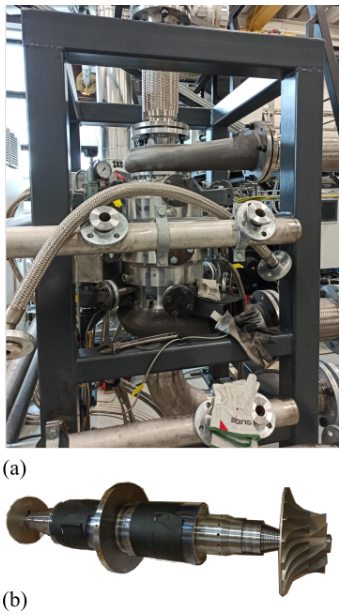

FIGURE 9. Experimental setup: (a) compressor, (b) permanent magnet rotor with compressor wheels.

Output sensitivities are almost the same for both fixed-parameter and LPV controllers, and thus, only the worst output sensitivity function of the four single-input single-output (SISO) loops is shown for the system with the fixed-parameter H_∞ controller applied to the plant at maximum speed (which is the worst case). The results indicate that the controllers withstand the gain uncertainty well.

Next, the time-domain performance is studied by comparing the measured and simulated radial positions during start-up from the safety bearings in Fig. 11. The controller has no integral action, and therefore, a small steady-state error in position after the settling time is observed. Further, because

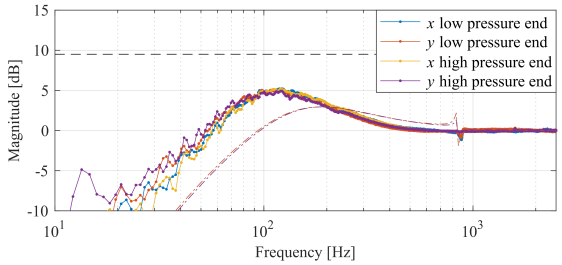

FIGURE 10. Measured and analytical output sensitivities computed one loop at a time for four SISO loops for the fixed-parameter H_∞ controller (synthesized with the LMI method for low speed) tested at high speed. Analytical output sensitivities are shown with the dash-dotted lines, measured sensitivities with the solid lines, and the 9.5dB limit with the dashed line.

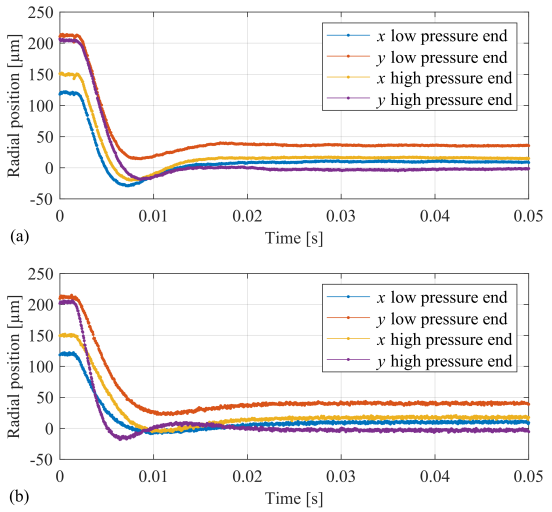

FIGURE 11. Measured and simulated radial positions during start-up from the safety bearings. (a) Measured, (b) simulated.

of the assembly inaccuracies and runout, the rotor is seen as in an eccentric position. In order to match the simulation results with the measured ones, an eccentricity vector [$x_{\mathrm{e,LP}}$ $y_{\mathrm{e,LP}}$ $x_{\mathrm{e,HP}}$ $y_{\mathrm{e,HP}}$] = [-11 -80 -22 30] μm was added to the simulation model.

V. CONCLUSIONS

Two robust control methods, i.e., fixed-parameter H_∞ control and LPV H_∞ control, were implemented based on the FEM plant model and applied to the bearingless compressor operating as part of a high-temperature 0.5 MW industrial heat pump for the first time. The time- and frequency-domain responses of the closed-loop system were used to evaluate the performance of the two control approaches. In addition, the RIC and LMI control synthesis methods were compared. The solution for the noncollocation problem was presented and tested using the estimated rotor position at bearing locations with the RIC method and the reconstructed position at bearing locations through rigid body transformation matrices with the LMI method. The positions estimated by the controller, computed with the RIC method, retain the correct information about the contribution of the bending rotor modes to the rotor deformation and thereby the displacement at bearing locations. This provides slightly better closed-loop performance indices than the controller computed with the LMI method. However, the LMI is suitable for the LPV control.

For rotors that are not highly gyroscopic, the LPV approach still provides better H_∞ norms compared with the fixed-parameter control. The LPV control has better performance in terms of closed-loop responses to noise at frequencies corresponding to the rotor bending mode frequencies. For the synthesis of fixed-parameter H_∞ controllers, the optimal speed point is generally closer to zero and not to the nominal rotor speed. For highly gyroscopic rotors, the LPV approach shows increasingly improved performance and robustness with higher rotational speeds.

Additionally, two different implementation methods for the linearization and motor current dependence decoupling of the magnetic forces have been tested in the simulations.

As constructions and control of bearingless machines continue to evolve, more avenues are opening for new high-power high-speed bearingless rotor applications and expanding research interests in the field.

VI. ACKNOWLEDGMENTS

Authors would like to thank Prof. Ioan-Dore Landau, Prof. Akira Chiba, and Asst. Prof. Niko Nevaranta for their valuable advice at different stages of this work. The technical team of LUT Voima and the research group of Fluid Dynamics at LUT under Prof. Teemu Turunen-Saaresti are also acknowledged. This work was supported by Business Finland: "EMBER High-temperature high-efficiency oil-free heat pump," no. 1745/31/2020, Tohtoristipendi 2021 at LUT, Suomen Kulttuurirahasto grant no. 00211193, the Academy of Finland under grants no. 350880 and 304784.

REFERENCES

[1] J. Chen, J. Zhu, and E. L. Severson, "Review of bearingless motor technology for significant power applications," IEEE Transactions on Industry Applications, vol. 56, no. 2, pp. 1377–1388, 2020.

[2] Z. Liu, A. Chiba, Y. Irino, and Y. Nakazawa, "Optimum pole number combination of a buried permanent magnet bearingless motor and test results at an output of 60 kW with a speed of 37000 r/min," IEEE Open Journal of Industry Applications, vol. 1, pp. 33–41, 2020.

[3] R. P. Jastrzebski, P. Jaatinen, H. Sugimoto, O. Pyrhönen, and A. Chiba, "Design of a bearingless 100 kW electric motor for high-speed applications," in 2015 18th International Conference on Electrical Machines and Systems (ICEMS), 2015, pp. 2008–2014.

[4] D. Kepsu, R. P. Jastrzebski, and O. Pyrhönen, "Modeling of a 30 000 rpm bearingless SPM drive with loss and thermal analyses for a 0.5 MW high-temperature heat pump," IEEE Transactions on Industry Applications, vol. 57, no. 6, pp. 6965–6976, 2021.

[5] G. Valente, A. Formentini, L. Papini, C. Gerada, and P. Zanchetta, "Performance Improvement of Bearingless Multisector PMSM With Optimal Robust Position Control," IEEE Transactions on Power Electronics, vol. 34, no. 4, pp. 3575–3585, 2019.

[6] W. Zhang, H. Zhu, Y. Xu, and M. Wu., "Direct Control of Bearingless Permanent Magnet Slice Motor Based on Active Disturbance Rejection Control," IEEE Transactions on Applied Superconductivity, vol. 30, no. 4, pp. 1–5, 2020.

[7] R. P. Jastrzebski and R. Pollanen, "Centralized optimal position control for active magnetic bearings: comparison with decentralized control," Electr Eng, vol. 91, no. 62, p. 101–114, 2009.
[8] N.-C. Tsai, C.-H. Kuo, and R.-M. Lee, "Regulation on radial position deviation for vertical AMB systems," Mechanical Systems and Signal Processing, vol. 21, no. 7, pp. 2777–2793, 2007.
[9] R. P. Jastrzebski, K. M. Hynynen, and A. Smirnov, "H-inf control of active magnetic suspension," Mechanical Systems and Signal Processing, vol. 24, no. 4, pp. 995–1006, 2010.
[10] C. Lusty and P. Keogh, "Active Vibration Control of a Flexible Rotor by Flexibly Mounted Internal-Stator Magnetic Actuators," IEEE/ASME Transactions on Mechatronics, vol. 23, no. 6, pp. 2870–2880, 2018.
[11] K. Glover and J. C. Doyle, "State-space formulae for all stabilizing controllers that satisfy an H_∞ norm bound and relations to risk sensitivity," Systems & Control Letters, vol. 11, no. 8, pp. 167–172, 1988.
[12] P. Gahinet, "Explicit controller formulas for LMI-based H_∞ synthesis," Automatica, vol. 32, pp. 1007–1014, March 1996.
[13] A. Morsi, H. S. Abbas, S. M. Ahmed, and A. M. Mohamed, "Model Predictive Control Based on Linear Parameter-Varying Models of Active Magnetic Bearing Systems," IEEE Access, vol. 9, pp. 23 633–23 647, 2021.
[14] A. Forrai, T. Ueda, and T. Yumura, "Electromagnetic Actuator Control: A Linear Parameter-Varying (LPV) Approach," IEEE Transactions on Industrial Electronics, vol. 54, no. 3, pp. 1430–1441, 2007.
[15] C. Poussot-Vassal, O. Sename, L. Dugard, P. Gáspár, Z. Szabó, and J. Bokor, "A new semi-active suspension control strategy through LPV technique," Control Engineering Practice, vol. 16, no. 12, pp. 1519–1534, 2008.
[16] H. Balini, J. Witte, and C. W. Scherer, "Synthesis and implementation of gain-scheduling and LPV controllers for an AMB system," Automatica, vol. 48, no. 3, pp. 521–527, 2012.
[17] F. Wu, "Switching LPV control design for magnetic bearing systems," in Proceedings of the 2001 IEEE International Conference on Control Applications (CCA'01) (Cat. No.01CH37204), 2001, pp. 41–46.
[18] A. Smirnov, R. P. Jastrzebski, and K. M. Hynynen, "Gain-scheduled and linear parameter-varying approaches in control of active magnetic bearings," in Proceedings of the Twelfth International Symposium on Magnetic Bearings (ISMB12), Wuhan, China, 2010, pp. 350–360.
[19] S. Mason, P. Tsiotras, and A. P, "Linear Parameter Varying Controllers for Flexible Rotors Supported on Magnetic Bearings," in Proceedings of the sixth International Symposium on Magnetic Bearings (ISMB6), 1998, pp. 341–351.
[20] B. Lu, H. Choi, G. D. Buckner, and K. Tammi, "Linear parameter-varying techniques for control of a magnetic bearing system," Control Engineering Practice, vol. 16, no. 10, pp. 1161–1172, 2008.
[21] H. Atoui, O. Sename, V. Milanes, and J. J. Martinez, "Smooth Switching of Multi-LPV Control Systems Based on Youla-Kucera Parameterization," IFAC-PapersOnLine, vol. 55, no. 35, pp. 19–24, 2022, 5th IFAC Workshop on Linear Parameter Varying Systems LPVS 2022.
[22] M. Wang, M. Cole, and P. Keogh, "New LMI based gain-scheduling control for recovering contact-free operation of a magnetically levitated rotor," Mechanical Systems and Signal Processing, vol. 96, pp. 104–124, 2017.
[23] J. Che, Y. Zhu, D. Zhou, and X. He, "Active fault tolerant control design using switching linear parameter varying controllers with inexact fault-effect parameters," International Journal of Robust and Nonlinear Control, vol. 32, no. 7, pp. 4477–4494, 2022.
[24] A. Zhuravlev and R. P. Jastrzebski, "Linear parameter-varying H_∞ control of bearingless machine," The 18th International Symposium on Magnetic Bearings, pp. 257–262, 2023.
[25] A. Zhuravlev, R. P. Jastrzebski, and L. Chechurin, "Numerical study of robust control for an AMB rotor with uncertain speed," 2022 IEEE/ASME International Conference on Advanced Intelligent Mechatronics (AIM), pp. 1799–1806, 2022.
[26] R. P. Jastrzebski, P. Jaatinen, O. Pyrhönen, and A. Chiba, "Design of 6-slot inset PM bearingless motor for high-speed and higher than 100kW applications," in 2017 IEEE International Electric Machines and Drives Conference (IEMDC), 2017, pp. 1–6.
[27] ——, "Current injection solutions for active suspension in bearingless motors," in 2017 19th European Conference on Power Electronics and Applications (EPE'17 ECCE Europe), 2017, pp. P.1–P.8.
[28] D. Kepsu, E. Kurvinen, J. Tiainen, J. Honkatukia, T. Turunen-Saaresti, and R. P. Jastrzebski, "Interdisciplinary design of a high-speed drivetrain for a kinetic compressor in a high-temperature heat pump," IEEE Access, vol. 9, pp. 143 877–143 900, 2021.
[29] J. Pyrhonen, V. Hrabovcova, and S. R. Semken, Electrical Machine Drives Control: An Introduction. Wiley, 2016.
[30] J. C. Doyle, K. Glover, P. Khargonekar, and B. Francis, "State-space solutions to standard H_2 and H_∞ control problems," IEEE Transactions on Automatic Control, vol. 34, no. 8, p. 831–847, 1989.
[31] O. Sename, P. Gaspar, and J. E. Bokor, Robust Control and Linear Parameter Varying Approaches: application to Vehicle Dynamics. Springer, 2013, vol. 437.

ANDREI ZHURAVLEV is a doctoral student at the LUT School of Energy Systems, Lappeenranta–Lahti University of Technology LUT. He received the Master's degree in a double degree program between LUT and Saint Petersburg Electrotechnical University (LETI). He completed his exchange studies in Zhejiang Ocean University, China. His field of interests is control of active magnetic bearings and bearingless machines.

ATTE PUTKONEN received the M. Sc. (Tech.) degree in electrical engineering from Lappeenranta–Lahti University of Technology LUT, Finland, in 2020. Currently, he is a doctoral student at the LUT School of Energy Systems. His research interests are identification and control of bearingless machines and active magnetic bearing systems.

SADJAD MADANZADEH received the B.S. degree in electrical engineering from the University of Zanjan, Zanjan, Iran, in 2010, and the M.S. degree in electrical engineering from the K. N. Toosi University of Technology, Tehran, Iran, in 2013. He is currently a researcher with Lappeenranta University of Technology, Lappeenranta, Finland. His research interests include electric drives control, electrical machine design, and power electronics.

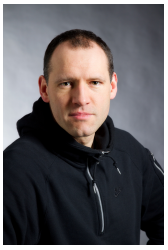

RAFAL P. JASTRZEBSKI received the M.Sc. degree in microelectronics from the Technical University of Lodz, Poland, in 2002, and the D.Sc. degree in electrical engineering from Lappeenranta University of Technology (LUT), Finland, in 2007. Currently, he is an Associate Professor (tenured) at the University of Turku and Docent with LUT University. His research interests include mechatronic systems, digital control, energy applications, active magnetic bearings, magnetic levitation systems, and bearingless machines. From 2013 to 2018, he was an Academy Research Fellow. From 2009 to 2011, he served as an Academy of Finland Postdoctoral Researcher.